TTMP vol 2 (1), 2025
doi: 10.30511/ttmp.2025.2053798.1048

Transactions in Theoretical and Mathematical Physics

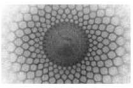

Crypto-Fiat Exchange Rates Network as indicator of macroeconomic dynamics

Y. Shahmari[1a], **H. Zare**[2b], **H. Hatami**[1c], **S. Rouhani**[3d]

[1] Physics Department, Sharif University of Technology, Tehran PO Box 11155-9161, Iran
[2] Department of Mathematical Sciences, Sharif University of Technology,P.O. Box 11155-9415, Tehran, Iran
[3]Physics Department and Research Center for High Energy Physics, Sharif University of Technology, Tehran PO Box 11155-9161, Iran

Received: 18 February 2025 / Accepted: 27 February 2025 / Published: 27 February 2025

Abstract The relationship between cryptocurrencies and fiat currencies reflects the dynamic connection between them, shaped by investors, macroeconomic forces, regulatory frameworks etc. In this article, we have shown how markets have evolved from a Bitcoin-centric ecosystem to a more Interconnected network, reflecting broader changes in the maturity of the financial system and geopolitical strategies

1 Introduction

A fundamental question in the crypto markets is: which cryptocurrency is the driver of the market movements? The immediate response may be that Bitcoin is the leader and other cryptos follow. A similar question in fiat currencies would be whether the Euro follows the Dollar or vice versa. We have attempted to answer these questions by looking at the Crypto/fiat exchange rates across diverse geographic markets and cryptocurrencies. There exist many crypto-fiat exchanges, where one may buy or sell cryptocurrencies. They facilitate conversion and transfer between traditional currencies (fiat) and cryptocurrencies, in such exchanges, these conversion rates are quoted and the rates change with time rapidly. This is certainly not exclusive to a single platform and may take other forms. However, such exchanges occur on a large scale. So we may think of a network of crypto/fiat pairs affecting the exchange rate of other such pairs. There is a question about the main drivers of pair exchange rates. Some good guesses exist in the market that surely bitcoin is the driver since it enjoys the largest circulating capital, high liquidity, and market dominance. However, this is not always the case. If you think of such an exchange rate as a stochastic time series, we face a deeper question of what we mean by calling a stochastic process the main driver node of the network of all crypt-fiat pairs. There are various ways of finding the driver and the derived between two-time series[1][2][3] but each of them has its flaws. We may examine the cross-correlation between the two rates at the simplest level. This leaves us with a correlation matrix. The returns can be expressed as a linear combination of uncorrelated (neither necessarily independent) random variables, using the eigenvectors of this matrix. The eigenvalues correspond to the squared volatilities of these components. However, In the case of Gaussian returns, the principal components are independent.
Estimating of full correlation matrix with empirical data is tough. This is depicted by the empirical spectrum of eigenvalues in the correlation matrix, against a completely random correlation matrix for which the analytic form is derived for large dimensions. The rates as a whole are in simple terms reflected by the largest eigenvalues while most eigenvalues can be attributed to a purely random correlation matrix. Volatility correlations cannot be described in terms of factor models either. There are many methods for the construction of arbitrarily correlated non-Gaussian random variables, and each of them is associated with different multivariate distribution.[4–6]
By constructing the maximal spanning tree, we can talk about the dominance of the main cluster. The central node of that main cluster can be regarded as the main driver of the network. Then, we can talk about the stability of the network using the largest eigenvalue and the spectral gap of the system. These results can be used to find the noise-dominated vs. signal-dominated parts of the network over time.

Our analysis yields three main contributions: (1) The existence of community leadership roles in cryptocurren-

[a]e-mail: Shahmari.acer@physics.sharif.edu
[b]e-mail: Hooman.zare99@sharif.edu
[c]e-mail: Hanie.hatami@physic.sharif.edu
[d]e-mail: (Corresponding author) srouhani@sharif.edu

cies that conflict the Bitcoin supremacy; (2) the signs of geo-distributed fiat currency activities signaling regional market integration; (3) Exposure of the critical thresholds where the network is resilient/impermeable through spectral/MST stability metrics, representing phase-transition behavior in market topology.

2 Methods

2.1 Data and Sources

The data used in this study consists of time-series data on prices, returns, market capitalizations, and volumes of various crypto-fiat currency pairs. [Appendix Appendix A] Two distinct datasets were utilized:

- Historical data from November 9, 2017, to August 21, 2022.
- Recent data from May 23, 2023, to August 19, 2024.

The data was gathered using the CoinGecko API and data center. The time-series data includes daily exchange rates and returns for each currency pair. The historical data required minimal preprocessing, with only a few instances of missing or NaN values corrected by carrying forward the previous values. The newer data contained no missing or NaN values.

2.2 Correlation Analysis

The Pearson correlation coefficient ρ between two time series X and Y is calculated as:

$$\rho_{XY} = \frac{\mathrm{cov}(X,Y)}{\sigma_X \sigma_Y} = \frac{\sum_{i=1}^{n}(X_i - \bar{X})(Y_i - \bar{Y})}{\sqrt{\sum_{i=1}^{n}(X_i - \bar{X})^2}\sqrt{\sum_{i=1}^{n}(Y_i - \bar{Y})^2}}, \quad (1)$$

where $\mathrm{cov}(X,Y)$ is the covariance of X and Y, and σ_X and σ_Y are the standard deviations of X and Y, respectively. The Pearson correlation coefficient was calculated to form a cross-correlation matrix ρ for each pair of crypto and fiat currencies. This matrix highlights the linear relationships between the daily returns of different currency pairs. The correlations were sorted and visualized to identify significant relationships. Although the cross-correlation matrix provides a snapshot of the relationships between currency pairs, it does not capture the temporal dynamics of these relationships.[7]

We are not interested in the global correlations of the market, because they miss the dynamics of observables of the market. A sliding window approach was employed to capture the temporal dependencies of correlations [8, 9]. For a given window size w, the moving correlation $\rho(t)$ at time t is computed using the data from $t - w$ to t. This results in a time series of correlations, illustrating how the relationships between currency pairs evolve. The decay could be modeled as a stochastic process affecting the entries of the correlation matrix.[10]

Using the sliding window method, we expect the determination of covariances to be noisy, and therefore the empirical correlation matrix to be to a large extent random, i.e. the structure of the matrix to be dominated by measurement noise. This is because for M time-series, the correlation matrix contains $M(M-1)/2$ entries, which must be determined from M time-series of length N. For the rolling window, N is considerably close to M.

2.3 Eigenvalue Analysis

Eigenvalues capture the key elements of a matrix. In random matrix theory (RMT), the Marchenko-Pastur distribution describes the eigenvalues of a random matrix [11]. Meaning that if the time series are continuous and independently, identically distributed (i.i.d.), the eigenvalues of the correlation matrix follow this distribution. But, in the case of crypto-fiat pairs, time-series consisted of a fixed crypto and varying fiats are far from independent and it is well known in the literature that the returns of economic time series are jumpy [12], hence discontinuous [13]. This means that we need to construct a new theorem for the crypto-fiat time-series.

The largest eigenvalue (λ_{max}) usually corresponds to the market mode, explaining the maximum variance [14]. In crypto-fiat markets, the largest eigenvalues are indicators of a dominant currency or overall market sentiment. The smallest eigenvalues (λ_{min}) however, relate to specific, maybe anti-correlated pairs and finds the fastest modes and fastest responses of the system. In traditional RMT, the bulk eigenvalues are semicircle (Wigner) or Marchenko-Pastur [15], but we will argue that the power law distribution of eigenvalues are more from heavy-tailed data or scale-free networks.

2.4 Non-Gaussian returns

If the returns are non-Gaussian we need to construct non-Gaussian correlated variables. Bouchaud et. al. [16] showed that correlated Gaussian variables can be transformed as a linear superposition of independent random Gaussian variables.

Let independent non-Gaussian factors F_a with distributions $P_a(f_a)$ be linearly combined as:

$$X_i = \sum_{a=1}^{M} b_{a,i} f_a, \tag{2}$$

where $b_{a,i}$ is a basis matrix diagonalizing the correlation matrix of X_i. The inverse transform is:

$$f_i = \sum_{i=1}^{M} b_{a,i} X_a. \tag{3}$$

$P_a(f_a)$ can be any arbitrary probability density function. An interesting case is when $P_a(f_a)$ is scale free:

$$P_a(f_a) \approx \lim_{|f_a|\to\pm\infty} \frac{\mu A_{a,\mu}}{|f_a|^{1+\mu}}. \tag{4}$$

Here, the variables X_i inherit tails with exponent μ and amplitude:

$$A_i^{\mu} = \sum_{a=1}^{M} |b_{ai}|^{\mu} A_a^{\mu}. \tag{5}$$

For Lévy stable factors ($\mu < 2$), X_i become multivariate Lévy variables.

We can involve non-linear transformations of correlated Gaussian variables. Let's define:

$$\tilde{X}_i = \sum_{a=1}^{M} b_{ai} f_a, \quad \text{with} \quad f_a \sim \mathcal{N}(0,1), \tag{6}$$

and map these to non-Gaussian variables via $X_i = G_i(\tilde{X}_i)$. The marginals $P_i(X_i)$ are enforced using:

$$P_i(X_i) = P_G(\tilde{X}_i) \left| \frac{d\tilde{X}_i}{dX_i} \right|, \tag{7}$$

where P_G is the Gaussian density. This corresponds to a Gaussian copula framework. Generalizing, let $u_i = P_{i<\text{arbitrary number}}(X_i)$, where $P_{i<}$ is the cumulative distribution of X_i. The copula $C(u_1, \ldots, u_N)$, defined as the joint distribution of u_i, isolates dependency structures. The inverse reconstruction is:

$$X_i = P^{-1}_{i<\text{same arbitrary number}}(u_i). \tag{8}$$

The next step is to incorporate stochastic volatility. Consider:

$$X_i = g \sum_{a=1}^{M} b_{ai} \tilde{f}_a, \tag{9}$$

where $\tilde{f}_a$ are Gaussian factors and g which is a common volatility factor follows an inverse gamma distribution. This generates multivariate Student's t-distributed returns.

To find out whether the linear model is better or not, we need to find a comparison metric. Define generalized kurtosis metrics; For the linear model, transform factors f_a to Gaussians $\tilde{f}_a = G_a^{-1}(f_a)$ and we compute:

$$K_{ab} = \langle \tilde{f}_a^2 \tilde{f}_b^2 \rangle - \langle \tilde{f}_a^2 \rangle \langle \tilde{f}_b^2 \rangle - 2\langle \tilde{f}_a \tilde{f}_b \rangle^2, \tag{10}$$

averaging over factor pairs:

$$\overline{K}_l = \frac{1}{M(M-1)} \sum_{a\neq b} K_{ab}. \tag{11}$$

For the non-linear model, map X_i to Gaussians $\tilde{X}_i = G_i^{-1}(X_i)$, we need to extract factors f_a, and compute:

$$\overline{K}_{nl} = \frac{1}{M(M-1)} \sum_{a\neq b} \left(\langle f_a^2 f_b^2 \rangle - \langle f_a^2 \rangle \langle f_b^2 \rangle \right). \tag{12}$$

Empirical tests yield $\overline{K}_{nl} = 0.221$ and $\overline{K}_l = 0.296$, favoring the Gaussian copula. Residual $\overline{K}_{nl}$ highlights unmodeled correlations from volatility fluctuations.

Dividing returns by the volatility proxy g (the "variety") reduces residuals to $\overline{K}_{nl} = 0.087$ and $\overline{K}_l = 0.066$. The model:

$$X_i = g \sum_{a=1}^{M} b_{ai} \tilde{f}_a, \tag{13}$$

with g diagonalizing volatility correlations, suppresses cross-kurtosis effectively.

While Gaussian copulas outperform linear non-Gaussian models[17], explicit volatility factors are critical for accurate dependency structures[18]. This aligns with the heavy-tailed, volatility-clustered nature of financial returns, favoring for models that integrate stochastic volatility.

2.5 Probability Distribution of Eigenvalues

In our case, correlation matrices are all symmetric. Hence, an ensemble of symmetric matrices with independent entries are required to find the noise component. Note that if there is any dominant mode for the system with meaningful information, the independence hypothesis will not hold, thus some eigenvalues will be outliers of the spectral density function we are going to derive. For any arbitrary random matrix A with finite variance and zero mean entries, we are interested in the family of $\{C_{M\times M} - A_{M\times M}\}_{A\in\mathbf{Sym}_{M\times M}(\mathcal{N}(0,.))}$ matrices where there exists at least one eigenvalue which is invariant upto finite fluctuations, a.s.

Let A be a symmetric random matrix of size $M \times M$ and its off-diagonal entries are i.i.d. random variables with zero mean and variance σ^2/M. The set of eigenvalues $\{\lambda_a\}_{a=1}^{M}$ of A satisfy eigenvalue equation:

$$A\boldsymbol{\nu}_a = \lambda_a \boldsymbol{\nu}_a. \tag{14}$$

We define the empirical spectral density as follows:

$$\rho_{empirical}(\lambda) := \frac{1}{M}\sum_{a=1}^{M}\delta(\mu - \mu_a), \tag{15}$$

where δ is a 1-point Dirac delta distribution function. Define resolvent $\mathcal{G}(\lambda)$ of A as:

$$\mathcal{G}_{ij}(\lambda) := ((\lambda\mathbf{I} - A)^{-1})_{ij}. \tag{16}$$

Where $\mathbf{I}$ is the identity matrix. Trace of the resolvent is connected to the eigenvalues with:

$$\mathbf{Tr}(\mathcal{G}(\lambda)) = \sum_{a=1}^{M}\frac{1}{\lambda - \lambda_a}. \tag{17}$$

By using Sokhotski–Plemelj theorem, we want to decompose the singular function $\frac{1}{x-i\epsilon}$ into its principal value and a Dirac delta function, meaning we can make a new representation for 1-point Dirac distribution functions that helps us to calculate $\rho_e(\lambda)$ at the limit $M \to \infty$.

For the limit $\epsilon \to 0$ for $\epsilon \in \mathcal{R}^+$, the Sokhotski–Plemelj theorem states:

$$\frac{1}{x - i\epsilon} = \mathcal{P}\frac{1}{x} + i\pi\delta(x), \tag{18}$$

where $\mathcal{P}\frac{1}{x}$ denotes the Cauchy principal value of $\frac{1}{x}$. This formula is useful in the study of spectral properties of operators, as it allows us to extract the imaginary part of the resolvent, which is directly related to the spectral density.

By adding a small imaginary part $i\epsilon$ to λ in equation (17) and applying the Sokhotski–Plemelj formula, we can isolate the imaginary part of the resolvent:

$$\frac{1}{\lambda - \lambda_a - i\epsilon} = \mathcal{P}\frac{1}{\lambda - \lambda_a} + i\pi\delta(\lambda - \lambda_a). \tag{19}$$

Taking the imaginary part of the trace of the resolvent, we obtain:

$$\Im\left[\mathrm{Tr}\,\mathcal{G}(\lambda - i\epsilon)\right] = \pi\sum_{a=1}^{M}\delta(\lambda - \lambda_a). \tag{20}$$

Thus, the spectral density can be written as:

$$\rho(\lambda) = \lim_{\epsilon\to 0^+}\frac{1}{M\pi}\Im\left[\mathrm{Tr}\,\mathcal{G}(\lambda - i\epsilon)\right]. \tag{21}$$

This expression connects the spectral density to the resolvent, providing a practical way to compute $\rho(\lambda)$ for large matrices.

Next step is constructing the recursive relation for resolvents, such that the empirical distribution $\rho_e(\lambda)$ approaches the spectral density of the random operator, a.s. Consider extending the matrix $A^{(M)}$ of size $M \times M$ to a larger matrix $A^{(M+1)}$ of size $(M+1)\times(M+1)$. The new matrix $A^{(M+1)}$ includes additional entries A_{0i} for $i = 1, \ldots, M$, and A_{00}. Note that the matrix A^{M+1} is symmetric, meaning that the elements A_{i0} have their respective couples in the A_{0i}.

The resolvent $\mathcal{G}^{(M+1)}(\lambda)$ of the extended matrix satisfies the following relation:

$$\frac{1}{\mathcal{G}_{00}^{(M+1)}(\lambda)} = \lambda - A_{00} - \sum_{i,j=1}^{M} A_{0i}A_{0j}\mathcal{G}_{ij}^{(M)}(\lambda). \tag{22}$$

This recursive formula allows us to compute the resolvent of the larger matrix $A^{(M+1)}$ in terms of the resolvent of the smaller matrix $A^{(M)}$. The key idea is to express the diagonal element $\mathcal{G}_{00}^{(M+1)}(\lambda)$ in terms of the elements of $\mathcal{G}^{(M)}(\lambda)$.

In the limit $M \to \infty$, the off-diagonal terms $\mathcal{G}_{ij}^{(M)}(\lambda)$ for $i \neq j$ become negligible, scaling as $\mathcal{O}(1/\sqrt{M})$. Additionally, the diagonal term A_{00} scales as $\mathcal{O}(1/\sqrt{M})$, so

it can be neglected compared to λ. This leads to the simplified recursion relation:

$$\frac{1}{\mathcal{G}_\infty(\lambda)} \approx \lambda - \sigma^2 \mathcal{G}_\infty(\lambda), \tag{23}$$

where σ^2 is the variance of the matrix elements. Solving this quadratic equation yields the limiting form of the resolvent $\mathcal{G}_\infty(\lambda)$, which is used to derive the spectral density $\rho(\lambda)$ in the large M limit. This yields:

$$\mathcal{G}_\infty(\lambda) = \frac{1}{2}\left(\frac{\lambda}{\sigma^2} - \sqrt{\frac{\lambda^2}{\sigma^4} - \frac{4}{\sigma^2}}\right). \tag{24}$$

This solution is chosen to ensure the correct behavior in the limit $\sigma \to 0$, where the resolvent reduces to $\mathcal{G}_\infty(\lambda) = \frac{1}{\lambda}$. The spectral density $\rho(\lambda)$ for $M \to \infty$ is given by:

$$\rho(\lambda) = \frac{1}{2\pi}\sqrt{4/\sigma^2 - \lambda^2/\sigma^4} \quad \text{for } (\lambda/\sigma)^2 \leq 4, \tag{25}$$

and zero otherwise. This is the well-known Wigner semi-circle law, which describes the distribution of eigenvalues of large symmetric random matrices.

Resolvent $\mathcal{G}_C(\nu)$ of the matrix C, can be written as:

$$\mathcal{G}_C(\nu) = \frac{\partial}{\partial \nu} \log\det(\nu \mathbf{I} - C). \tag{26}$$

Using the identity for the determinant of a symmetric matrix $\mathbf{X}$:

$$\det(\mathbf{X})^{-1/2} = \int \exp\left(-\frac{1}{2}\boldsymbol{\phi}^\top \mathbf{X} \boldsymbol{\phi}\right) \prod_{i=1}^{M} \frac{d\phi_i}{\sqrt{2\pi}}, \tag{27}$$

we express $\mathcal{G}_C(\nu)$ in terms of an integral over auxiliary variables $\boldsymbol{\phi}$. By averaging over the random matrix A performing a saddle-point approximation and using a replica trick to handle the quenched disorder arising from the randomness in A, we can find the spectrum density.

Let $C = AA^\top$, where A is an $M \times N$ matrix with independent and identically distributed (iid) entries of variance σ^2/N. The eigenvalues ν_a of C are related to those of A via $\nu_a = \lambda_a^2$.

For $M, N \to \infty$ with $c = N/M \geq 1$, the spectral density of C is given by:

$$\rho(\nu) = \frac{c}{2\pi\sigma^2}\sqrt{\frac{(\nu_{\max} - \nu)(\nu - \nu_{\min})}{\nu}}, \tag{28}$$

where the spectral edges are:

$$\nu_{\min}^{\max} = \sigma^2\left(1 + \frac{1}{c} \pm 2\sqrt{\frac{1}{c}}\right), \tag{29}$$

and $\nu \in [\nu_{\min}, \nu_{\max}]$. This is the Marčenko-Pastur distribution, which describes the eigenvalue distribution of large sample covariance matrices.

For finite N, the sharp edges of the spectral density become blurred. Let $\lambda_{\max/\min}^{(N)}$ denote the empirical extremal eigenvalues of C for finite N. Then:

$$\lim_{N\to\infty} \mathbb{P}\left(\lambda_{\max}^{(N)} > \nu_{\max}\right) = 0, \tag{30}$$

with a similar result holding for $\lambda_{\min}^{(N)}$. This means that, as N increases, the probability of finding eigenvalues outside the theoretical bounds $[\nu_{\min}, \nu_{\max}]$ vanishes.

2.6 Maximal Spanning Tree Algorithm

The maximal spanning tree (MST) graph is constructed based on the correlation matrix of crypto-fiat pairs [19]. Consider $M(M-1)/2$ entries of correlation matrix C from the daily returns of crypto-fiat pairs. First, rank the C_{ij} in descending order. Nodes of this tree are crypto-fiat pairs, and edges must be added iteratively from the decreasing list of C_{ij}. This process should be repeated for all the correlation entries, unless adding a link between the pair under consideration creates a loop in the graph, in which case skip that edge.

Once this process in finished, one finds a tree constructed based on the largest correlation values. This tree is named maximal spanning tree. Figure (2) finds the maximal spanning tree for two datasets, based on a fixed fiat. There are several methods to cluster MST and find the center node, but the figure is informative on its own.

2.7 Spectral Gap Analysis

Eigenvalues of correlation matrix C which is positive semi-definite, can be written in the following way:

$$\lambda_1 > \lambda_2 > \cdots > \lambda_M \geq 0. \tag{31}$$

From that, we can define spectral gap $\Delta\lambda$ as the difference between two largest eigenvalues.

$$\Delta\lambda := \lambda_1 - \lambda_2. \tag{32}$$

Mathematically, we can fix some bounds on $\Delta\lambda$. Since diagonal entries are all 1, $\mathbf{Tr}(C) = M$, meaning that $\sum_{i=1}^{M} \lambda_i = M$. For λ_1 we have:

$$\lambda_1 = M - \sum_{i=2}^{M} \lambda_i \tag{33}$$

For spectral gap, we get to the following relation:

$$\Delta\lambda = M - \lambda_2 - \sum_{i=2}^{M} \lambda_i. \tag{34}$$

We can find two bounds on $\Delta\lambda$. An upper bound can be found set λ_1, due to λ_2 being positive. A lower bound can be found by the using equation (31) on equation (34), getting to:

$$\Delta\lambda \geq M - \lambda_2 - (M-1)\lambda_2 = M(1-\lambda_2). \tag{35}$$

This lower bound is not necessarily negative, but since the eigenvalues are all positively sorted, the spectral gap is always positive.

For a large spectral gap, we can deduce that λ_2 is small, meaning that the largest cluster of data is due to one dominant eigenvalue. Using principle component analysis (PCA), λ_1 is variance explained by first principal component (PC1), and $\Delta\lambda$ is excess variance in PC1 over PC2. PCA can be regarded as intrinsic dimensionality of the whole data. By using PCA stability theorem, we can show that how much this system is stable.

First, consider $\tilde{C} = C + E$ to be a perturbed matrix with $\|E\|_2 < \frac{\Delta\lambda}{2}$. Let v_1 be the dominant eigenvector of C and $\tilde{v}_1$ of $\tilde{C}$. By the Davis-Kahan $\sin\theta$ theorem, the angle θ between v_1 and $\tilde{v}_1$ satisfies:

$$\sin\theta \leq \frac{\|E\|_2}{\Delta\lambda - \|E\|_2}. \tag{36}$$

Given $\|E\|_2 < \frac{\Delta\lambda}{2}$, the denominator $\Delta\lambda - \|E\|_2 > \frac{\Delta\lambda}{2}$. Thus:

$$\sin\theta \leq \frac{\|E\|_2}{\Delta\lambda/2} \implies \theta \leq \arcsin\left(\frac{2\|E\|_2}{\Delta\lambda}\right). \tag{37}$$

For small θ, $\sin\theta \approx \theta$, so $\|\tilde{v}_1 - v_1\|_2 \approx 2\sin(\theta/2) \leq \frac{2\|E\|_2}{\Delta\lambda}$. So the v_1 and $\tilde{v}_1$ are related by:

$$\|\tilde{v}_1 - v_1\|_2 \leq \frac{2\|E\|_2}{\Delta\lambda}. \tag{38}$$

Thus, a large $\Delta\lambda$ stabilizes v_1.
This result can be shown using the von neumann entropy. The von Neumann entropy is defined:

$$S(C) = -\sum_{i=1}^{n} \frac{\lambda_i}{n} \log \frac{\lambda_i}{n}. \tag{39}$$

Let $\lambda_1 = \frac{M}{M} + \frac{\Delta\lambda}{M} = 1 + \frac{\Delta\lambda}{M}$, and $\lambda_i = \frac{M-\Delta\lambda}{M(M-1)}$ for $i \geq 2$. Expanding $S(C)$:

$$\begin{aligned} S(C) = &- \frac{1+\frac{\Delta\lambda}{M}}{M} \log\left(\frac{1+\frac{\Delta\lambda}{M}}{M}\right) \\ &- \sum_{i=2}^{M} \frac{\frac{M-\Delta\lambda}{M(M-1)}}{M} \log\left(\frac{\frac{M-\Delta\lambda}{M(M-1)}}{M}\right). \end{aligned} \tag{40}$$

Using $\log(1+x) \approx x$ for small $\Delta\lambda/M$:

$$S(C) \approx \log M - \frac{\Delta\lambda}{M} + \mathcal{O}\left(\frac{\Delta\lambda^2}{M^2}\right). \tag{41}$$

Now, for a large $\Delta\lambda \gg \lambda_2$, we want to show the graph G with adjacency matrix C contains a dominant cluster.

By using the eigenvectors of C, we can find spectral clustering partitions G. By the Perron-Frobenius theorem, v_1 has non-negative entries and a large $\Delta\lambda$ implies v_1 dominates the spectrum, so its entries $v_1(i)$ reflect node's "importance." we can partition nodes via:

$$\begin{aligned} \text{Dominant cluster} &= \{i \mid v_1(i) \geq \tau\}, \\ \text{Outliers} &= \{i \mid v_1(i) < \tau\}, \end{aligned} \tag{42}$$

For a threshold τ, since $\lambda_2 \ll \Delta\lambda$, the residual eigenvalues $\lambda_2, \ldots, \lambda_n$ correspond to weak connections, justifying the partition.

For a random matrix C_{rand} with i.i.d. entries (mean 0, variance σ^2), Wigner's semicircle law states eigenvalues lie in $[-2\sigma\sqrt{M}, 2\sigma\sqrt{M}]$. Normalizing C as a correlation matrix (unit diagonal), $\sigma^2 = \frac{1}{M}$. The largest eigenvalue λ_1 of C_{rand} converges to $2\sqrt{M}$. If $\Delta\lambda = \lambda_1 - \lambda_2 > 2\sqrt{M}$, then $\lambda_1 > 2\sqrt{M}$, violating the random matrix threshold, implying structured correlations.

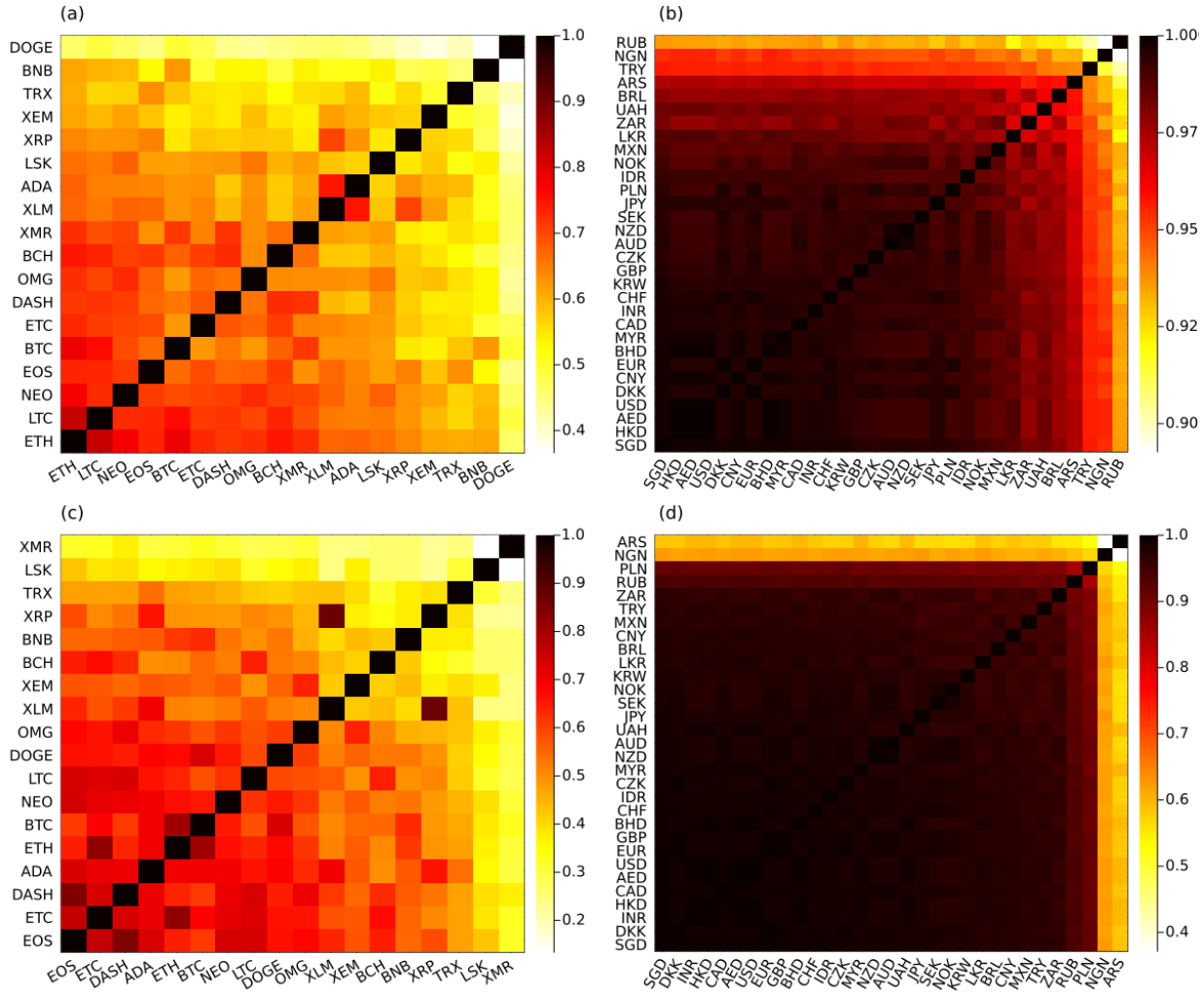

Fig. 1: Heatmap representations of the cross-correlation matrices computed from the daily returns of crypto–fiat pairs. Panels (a) and (b) correspond to the historical ("old") dataset, with panel (a) displaying correlations among cryptocurrencies in the USA market and panel (b) showing correlations among fiat currencies for BTC. Panels (c) and (d) show the corresponding matrices for the recent ("new") dataset.

3 Results

3.1 Cross-Correlation Analysis

3.1.1 Matrix Heatmap

The Pearson correlation coefficient (Eq. 1) quantifies linear relationships between pairs. Figure 1 presents heatmaps of cross-correlation matrices computed from daily returns of crypto(panels a and c) and fiat(panels b and d) pairs. The scores range from -1 (anti-correlation) to +1 (perfect correlation), which is shown by a color gradient (e.g., dark red for high positive correlations). During market stress, investors may sell riskier assets and buy safer ones, creating negative correlations. Wars, elections, or natural disasters can suddenly change market dynamics, causing temporary negative correlations. Due to this nature of markets, over short periods, correlations can fluctuate due to specific events or trends, and be negative, while long-term correlations are mostly stable and positive. For this reason, in Figure 1, which is calculated for a long period (2 to 4 years), negative correlation is not observed. Panels a and c elevated intra-crypto correlations (clustered red blocks) in USA market, and show that cryptocurrencies move together, driven by shared market drivers (e.g., ETH dominance). More recent data (panel c) may show higher correlations, reflecting clustered markets dynamics. In Panels b/d Fiat pairs exhibit high correlations, which can be powered by macro policy or geopolitical risk. Fiat pairs (like USD/EUR, JPY/PLN) tend to exhibit high correlation due to global economic conditions, High trading volumes, etc. The value of fiat currencies often moves in response to global economic con-

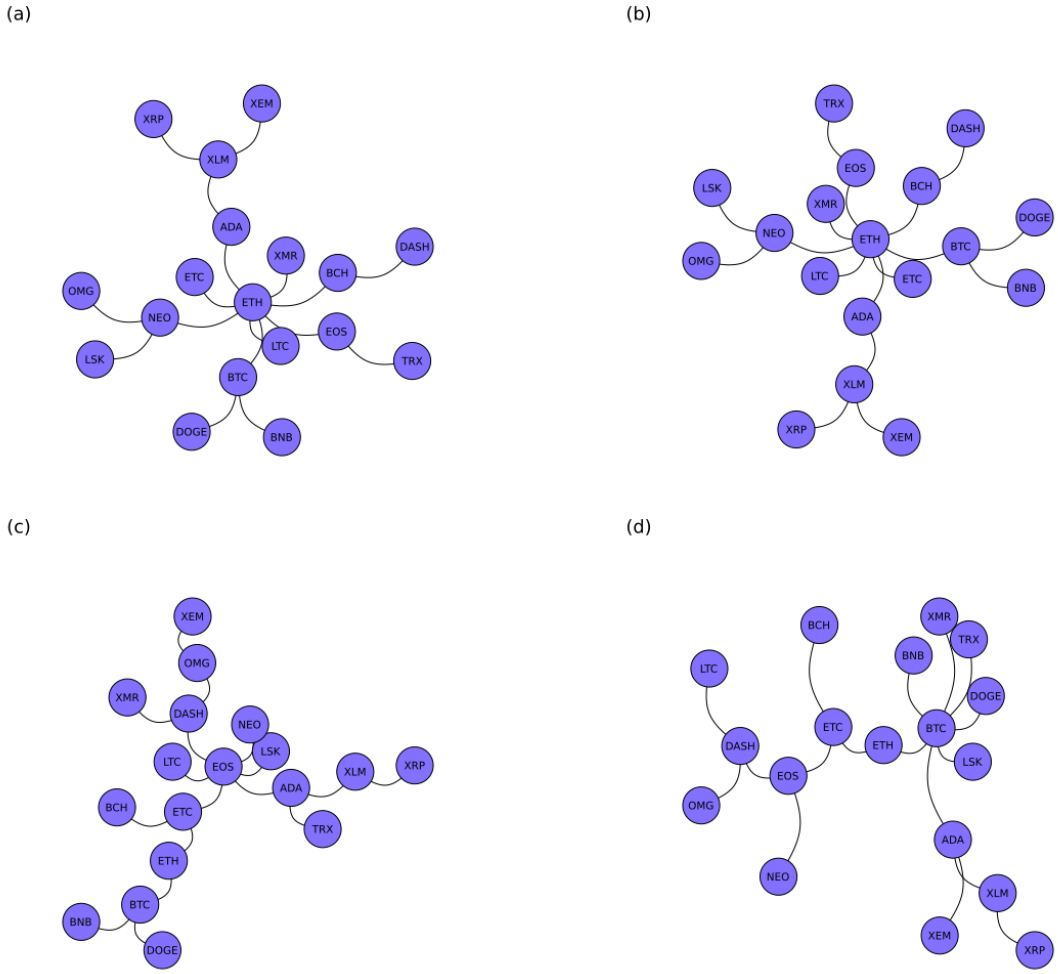

Fig. 2: Maximal spanning trees (MST) constructed from the correlation network of crypto–fiat pairs. Panels (a) and (c) depict the MST for the USD market based on the historical and recent datasets, respectively, while panels (b) and (d) show the MST for the ARS market. These trees highlight the strongest interdependencies and identify central nodes in each market.

ditions, which can affect the entire fiat market similarly. Also, high trading volumes in fiat pairs can lead to a more uniform price behavior across different fiats. These factors lead to more correlated fiats which demonstrated in panels b and d.

3.1.2 Correlation MST Graph

Figure 2 demonstrate MSTs for crypto–fiat correlation networks. Panels (a,c) and (b,d) represent USD and ARS markets for historical and recent datasets, respectively. Nodes in the graph represent crypto-USD or crypto-ARS (e.g., BTC-USD), while edges show the strongest correlations. Starting from the highest correlations, edges have been added one by one without loops (Section 2.6). The MST highlights the most important interdependencies. Recent data reflect decentralized structures when some altcoins, such as BNB, are in leading positions. Emerging markets like ARS (Argentine Peso) might exhibit the opposite in ETH-ARS, tight clustering around stablecoins as a hedge against hyperinflation. Ethereum(ETH) works its way to the central node of historical networks, given that it very often demonstrates high liquidity and hectic trading activity in a wide assortment of fiat currencies. The wide use of this cryptocurrency as the base or quote currency on many exchanges makes them have strong ETH-fiat pair statistical associations-a characteristic that simply makes them main candidates for primary links in any spanning tree. The central position of Ethereum(ETH) is further underlined by its more general use within the digital finance ecosystem, in particular in DeFi and tokenized asset markets. This wide utility, combined with market dynamics wherein ETH often plays the role of gateway

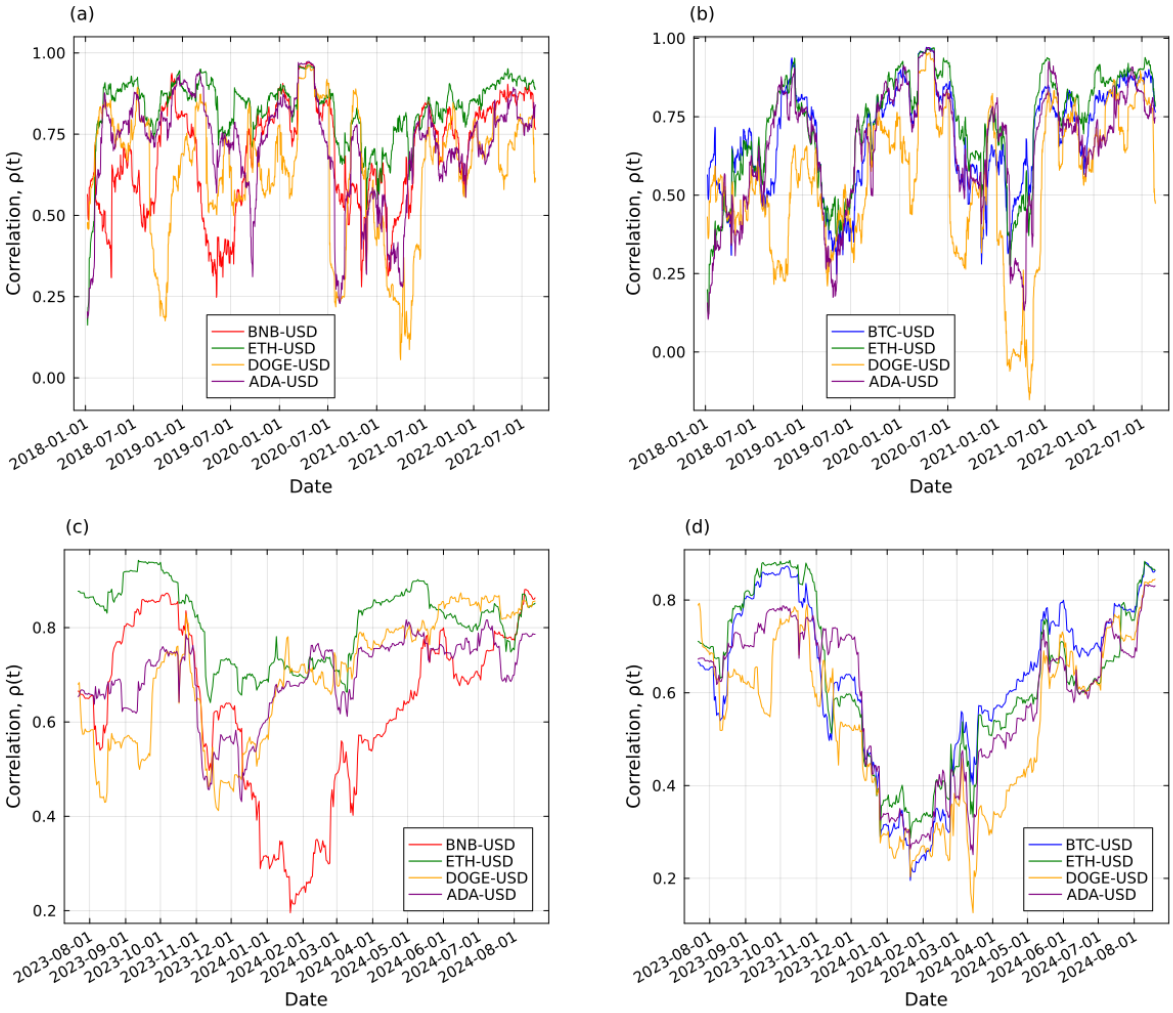

Fig. 3: Time evolution of moving correlations for key cryptocurrency pairs in the USD market. Panels (a) and (c) present the moving correlation of BTC–USD with a selection of other cryptocurrencies for the historical and recent datasets, respectively. Panels (b) and (d) show the analogous analysis for BNB–USD.

between traditional fiat systems and the wider crypto market, means it evidences consistently high connectivity across different fiat currencies. Because of that, when the maximal spanning tree algorithm underlines the most important relationships, ETH naturally takes the central position-actually bridging several fiat nodes and underlining its importance in the cryptocurrency ecosystem.

3.2 Dynamic Analysis

3.2.1 Moving Correlation Analysis of Crypto Currencies

Figures 3 (USD market) and 4 (CNY market) show time-evolving moving correlations between BTC/BNB and other cryptos. Panels (a/c) and (b/d) correspond to historical and recent datasets. Sliding window approach (Section 2.2) with window size w. Correlations fluctuate due to market events (e.g., Bitcoin halvings, regulatory announcements). In Figure 3 a and c, high correlations with major cryptos (ETH, LTC) persist but decline post-2023, indicating reduced Bitcoin hegemony. In Figure 3 b and d, increasing correlations with DeFi tokens (e.g., CAKE) reflect Binance Smart Chain's growth. In Figure 4 a and c, Sharp drops during China's crypto bans (2021) and rebounds after partial policy relaxations. In Figure 4 b and d, Lower correlations due to China's strict crypto regulations, isolating BNB from domestic markets.

3.2.2 Moving Correlation Analysis of Fiat Currencies

Figures 5 (BTC–fiat) and 6 (BNB–fiat) illustrate dynamic correlations between BTC or BNB and fiat currencies (USD, EUR, JPY, CNY). In Figure 5 a and c, low correlations during market crashes (e.g., COVID-19

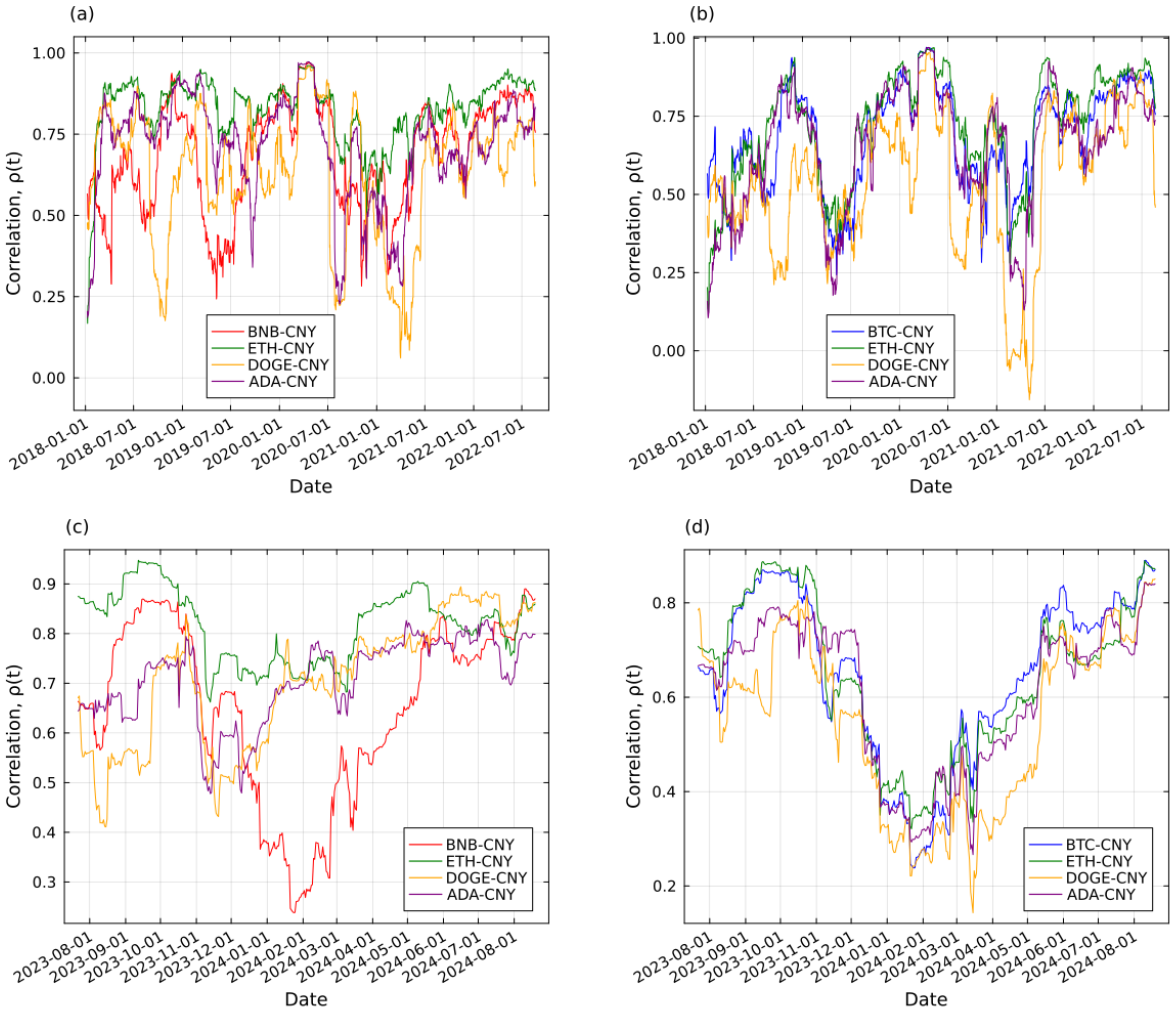

Fig. 4: Temporal moving correlations for crypto pairs in the CNY market. Panels (a) and (c) display the evolution of the moving correlation between BTC–CNY and selected cryptocurrencies for the historical and recent datasets, respectively, while panels (b) and (d) provide the corresponding analysis for BNB–CNY.

sell-off in 2020) as investors flee to USD. Recent data (panel c) shows weaker ties, suggesting decoupling from traditional markets. In Figure 5 b and d, anti-correlations during capital control tightening in China, with CNY devaluation driving crypto inflows. In Figure 6 a and c, rising correlations post-2023 mirror Binance's regulatory compliance in the U.S. In Figure 6 b and d, minimal linkage due to China's crypto bans, highlighting geographic fragmentation.

3.2.3 Eigenvalue Dynamics

In correlation matrices, eigenvalues quantify the variance (importance) of orthogonal factors. The largest eigenvalue (λ_{Max})(Figures 7 and 8) shows the market mode which explain the collective behavior of most assets. When λ_{Max} is large, it can be concluded that most assets are driven by a common force which can be anything like macroeconomic shocks or Bitcoin's price swings. In this situation a shock to one asset can propagate rapidly across the network.

During the 2018 crypto winter (long term market crash), Bitcoin's collapse dragged down altcoins which resulted to a spike in λ_{Max}. The 2021 Terra-Luna collapse increased panic selling cross crypto markets which further elevating λ_{Max}. Dampened (smaller) λ_{Max} in panel c shows reduction of dominance of a single market driver, this can be due to the increasing adoption of altcoins (e.g., Solana, Ripple) and decentralized finance(DeFi) tokens. Maturation of Regulation in these areas can also help to reduce the power of on dominant coin like Bitcoins. A spike in λ_{Min} (e.g., 2020-01-01) signals investors abandoning risky assets for safety. For example in 2020 COVID-19 Crash investors sold volatile cryptos like BTC and ETH and but stablecoins like USDT and USDC or fiats like

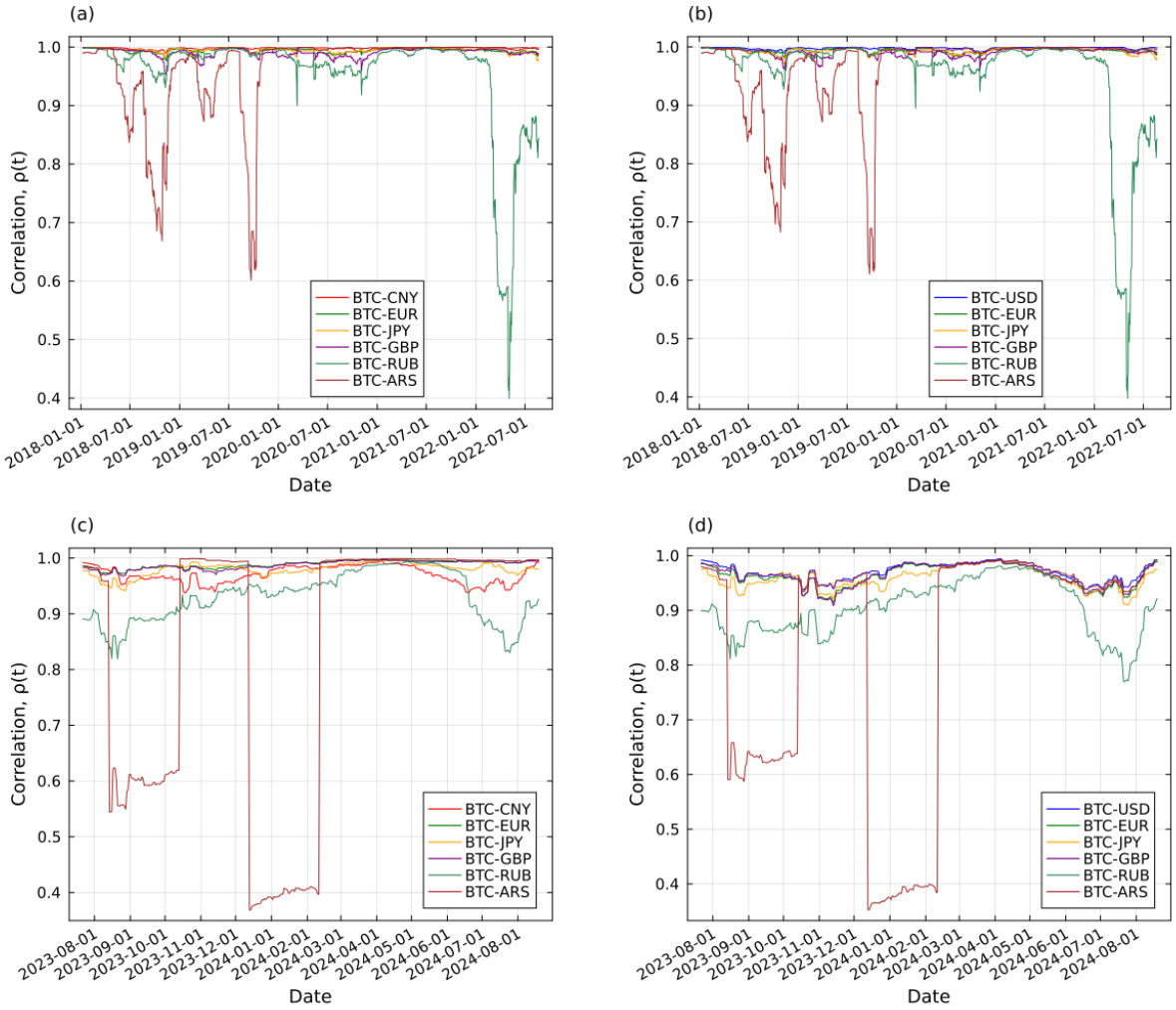

Fig. 5: Dynamic analysis of Bitcoin exchange rates with fiat currencies. Panels (a) and (c) illustrate the moving correlations between BTC–USD and a set of fiat currencies for the historical and recent datasets, respectively. Panels (b) and (d) show the moving correlation analysis for BTC–CNY with the same set of fiat currencies.

USD, creating anti correlation between risky and safe assts.

In the beginning of Russia-Ukraine war invasion (24th Feb 2022), Ruble (Russia's national currency) market experience a large increase in λ_{Max} and decrease in λ_{Min} which can demonstrate an unstable crypto-market in russia due to the uncertainty among people and selling cryptos to obtain safe money.

3.2.4 Spectral Analysis

In figure 9, panels a and c are for fixed crypto. The maximum of these frames are found in section 2.7 and for panels a and c are 31. The same value for the panels b and d (which are for fixed fiats and varying cryptos) is calculated to be 18. When the $\Delta\lambda$ is higher, it means that the overal system is more stable. When it reaches the maximum, this means that the system is effectively 1 dimentional, meaning that the mode of the network can be determined by only one time series. In section 2.7 we found that the $1:1$ signal to noise ratio can be found by $2\sqrt{M}$ which for fixed crypto (a and c), this number is 11.14 and for fixed fiats (b and d) this number is 8.49. When the spectral gap is above that value, the network is signal dominated and when the spectral gap is less than that, the noise is dominant. We expect to see some phases where crypto market is noise dominated, due to the independencies and local values of different coins. This can be seen in panels b and d, but with the same previously mentioned reasons like Russia-Ukraine war, we can see deviations for different fiats. For panels a and c, where a coin is fixed, we expect the healthy market to have a near maximal spectral gap. The market has been found in signal zone, which is exactly what we expect from non-isolated nations. If the price of one coin in some market,

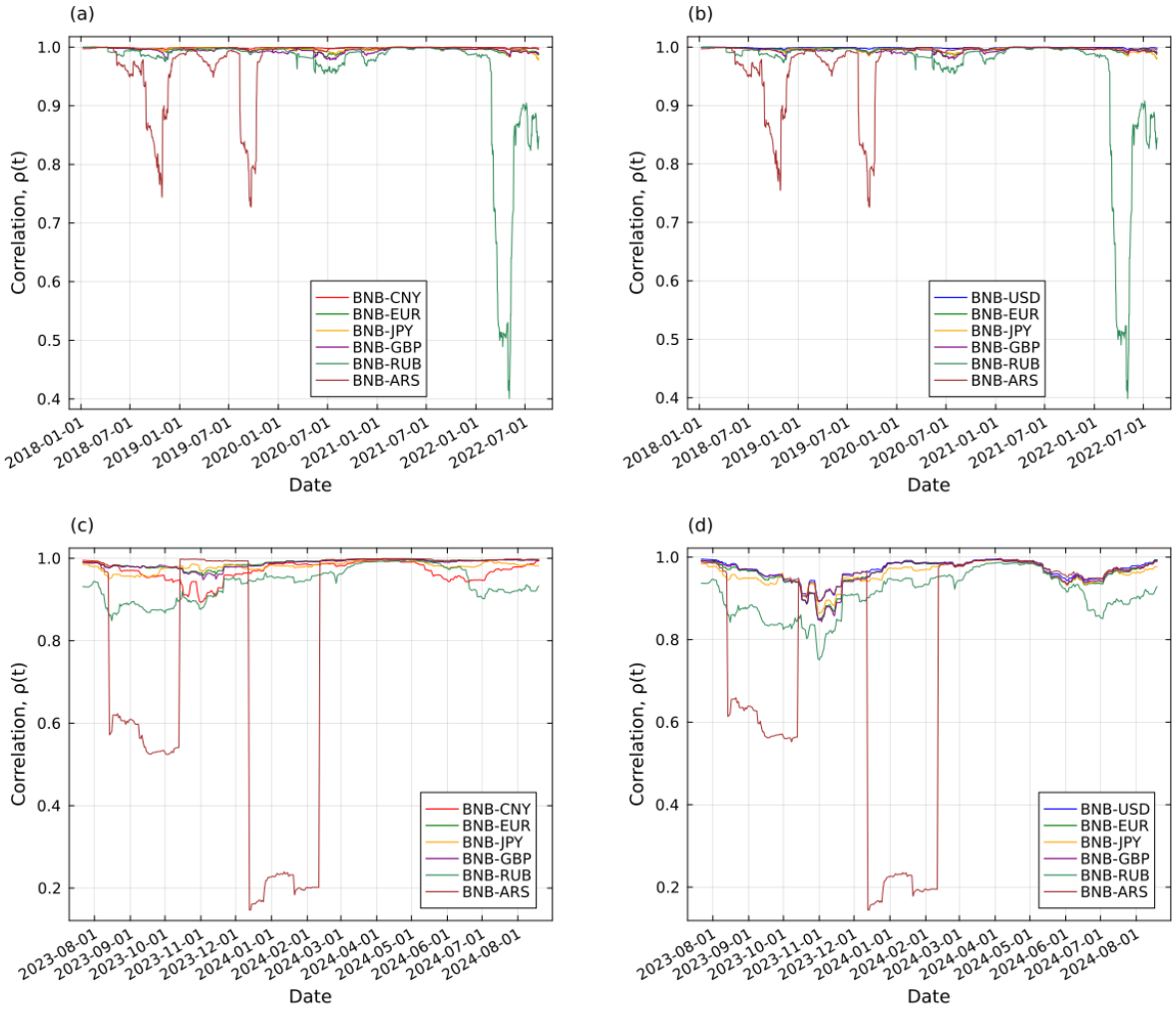

Fig. 6: Time evolution of moving correlations between Binance Coin (BNB) and fiat currencies. Panels (a) and (c) depict the moving correlations for BNB–USD for the historical and recent datasets, respectively, whereas panels (b) and (d) display the corresponding analysis for BNB–CNY.

for example BTC is totally independent from the price of the BTC in another market, we expect the spectral gap to get lower, hinting at possible separated communities, but since the change in the exchange rate between two fiats is slower that changes in cryptos, the independence of two exchange rates leads to different values of the same crypto in two fiats which easily gets exploited naturally. In figure 10, we can see the spectral gap of the overall network, consisted of all of the possible crypto-fiat pairs. The bound for being noise dominated can be calculated as 48.50, and the overall system is found to be always signal dominated, but it fluctuates.

3.2.5 Empirical Spectral Density

In figure 11, the histogram of eigenvalues are plotted in blue, and the redline is the eq 28 calculated for the dimension of the C. red line is only shifter vertically for better visualization. Since the scale of both frames are in Log-Log, vertical shift is a mere constant. In frame a, the value is calculated for older data, and in panel b this is calculated for newer data. The outlier λ_{max} is detected in both data sets, and for the newer data it has seen a notable shift to the right, meaning that the main cluster of the network is getting more fixed. There is another outlier in the small values that can be seen in the left part of both panels, which sets the fastest responses of the system. the smallest eigenvalue changes the eigenvector a lot (because there are many small eigenvalues and their respective eigenvector changes position as the pair of the leftmost eigenvalue). by changing eigenvectors, the fastest response of the system does not have a unique community.

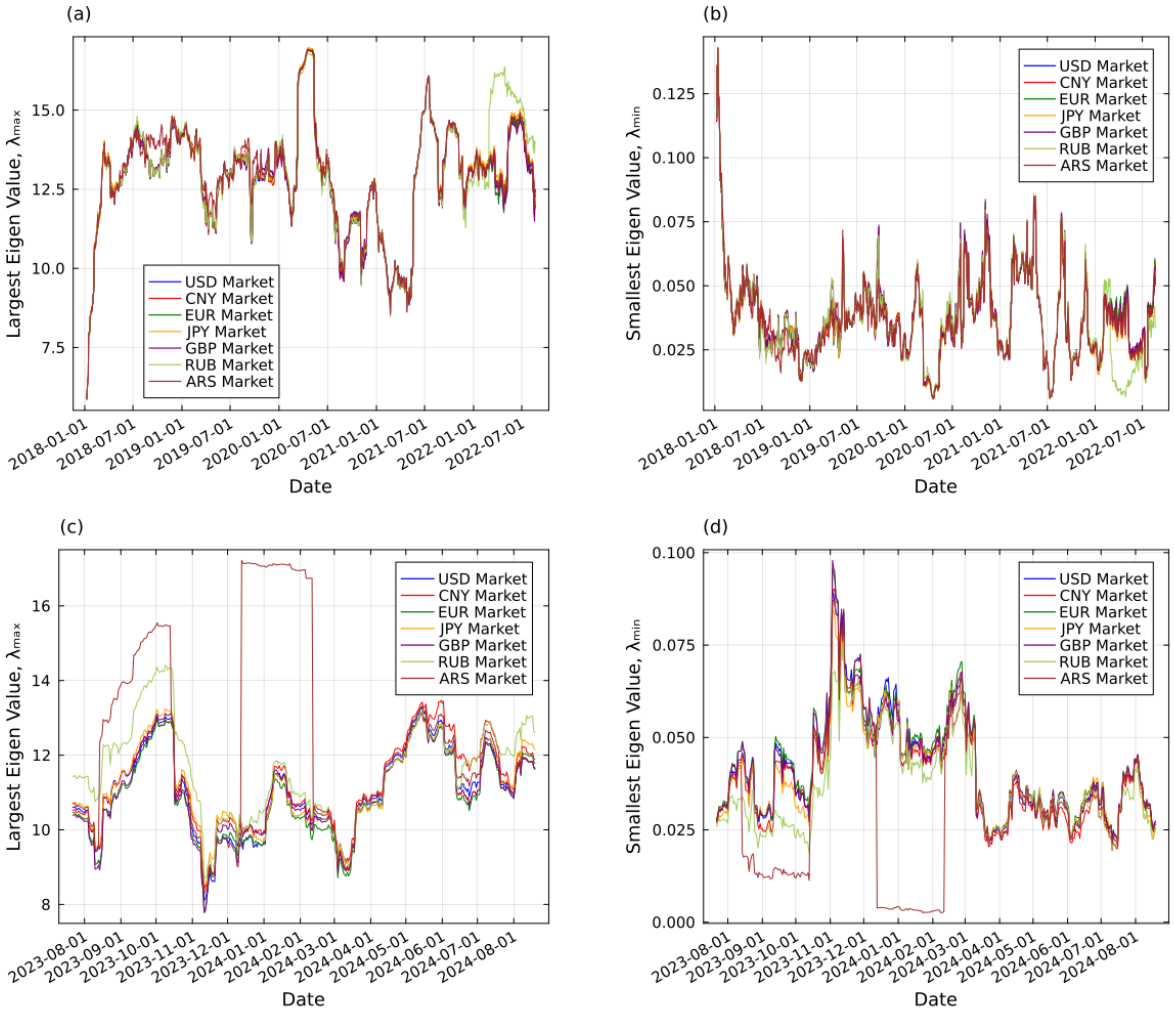

Fig. 7: Evolution of extreme eigenvalues from the fiat currency correlation matrices. Panels (a) and (c) show the time evolution of the largest eigenvalues (reflecting dominant market modes) for the historical and recent datasets, respectively, while panels (b) and (d) present the dynamics of the smallest eigenvalues (indicating fast responses of the system).

4 Discussion

The relationship between the cryptocurrencies and fiat currencies reflects the dynamic connection between them, shaped by investors, macroeconomic forces, regulatory frameworks, etc. In this article, we have shown how markets have evolved from a Bitcoin-centric ecosystem to a more interconnected network, reflecting broader changes in the maturity of the financial system and geopolitical strategies.[20] The shift in centrality from Bitcoin to Ethereum in the maximum spanning trees and Ethereum's high correlation in the markets underscores the historical shift in market power from digital gold to digital superpower in the cryptocurrency market.

During the early years (2017-2022), Bitcoin-USD acted as the main conduit for market sentiment.[21] However, in 2023-2024, Bitcoin's dominance declined significantly and Ethereum entered the game.[22] As the spectral gaps and maximum spanning trees indicate, this shift is aligned with the rise of the Ethereum DeFi ecosystem, regulatory scrutiny of Bitcoin mining (e.g., China's ban in 2021), and the emergence of seasonal cycles in which investors diversify into tokens like BNB and Solana.

The strong similarity between the USD and CNY markets illustrates how geopolitical tensions and regulatory policies make crypto-fiat networks well-suited to identifying arbitrage opportunities. China's tough stance on cryptocurrencies – which led to a mining and trading ban in 2021 – severed BTC-CNY correlations, directing capital flows toward stablecoins like USDT-ARS in inflation-prone economies (e.g., Argentina).[23] Emerging markets are increasingly prominent in the crypto-fiat network. In Turkey (TRY), crypto adoption increased during the 2023

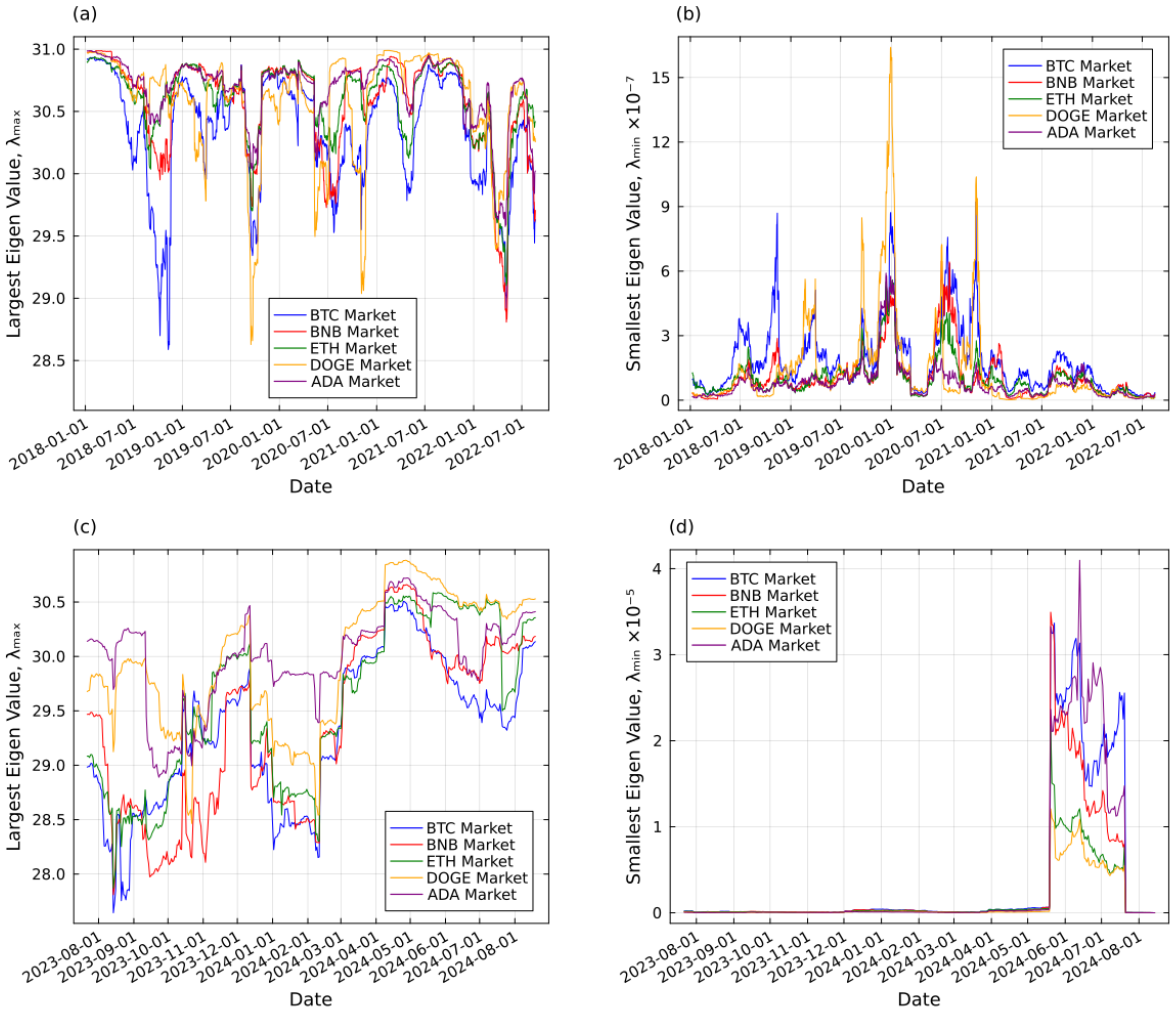

Fig. 8: Temporal evolution of extreme eigenvalues in the crypto currency correlation matrices. Panels (a) and (c) show the evolution of the largest eigenvalues, and panels (b) and (d) display the smallest eigenvalues, for the historical ("old") and recent ("new") datasets respectively, thus capturing shifts in overall market sentiment and specialized behavior.

currency crisis, and as citizens sought refuge in cryptocurrencies from the devaluation of the lira, the BTC-TRY correlation on the network increased.

The largest eigenvalue (λ_{Max}) peaked during economic crises (such as the 2018 crypto winter or the 2022 Terra-Luna collapse). The largest eigenvalue, which indicates the fast responses of the system to any noise, emphasizes the vulnerability of these sectors to leverage and bubbles. Notably, the deviation of the eigenvalue distributions from the Marchenko-Pastor rules (Section 2.3) highlights the inherent non-Gaussian nature of the crypto market.[24] The heavy-tailed returns and the microstructure-noise (created by retail buying and selling and their speculation in response to the media) make traditional portfolio models inadequate.[25]

While this paper greatly enhances our understanding of crypto-fiat networks, it has notable limitations. The inability to analyze causality is one of the problems with the Pearson correlation, which limits our ability to distinguish between leaders and followers in market movements. Relying on Pearson correlation also ignores nonlinear dependencies (due to group effects and the combination of multiple cryptocurrencies). We also encounter problems such as false edges or spurious edges when plotting the network using Pearson correlation.[26] Future research could address these problems by using mutual information or interaction-based models and polynomials.

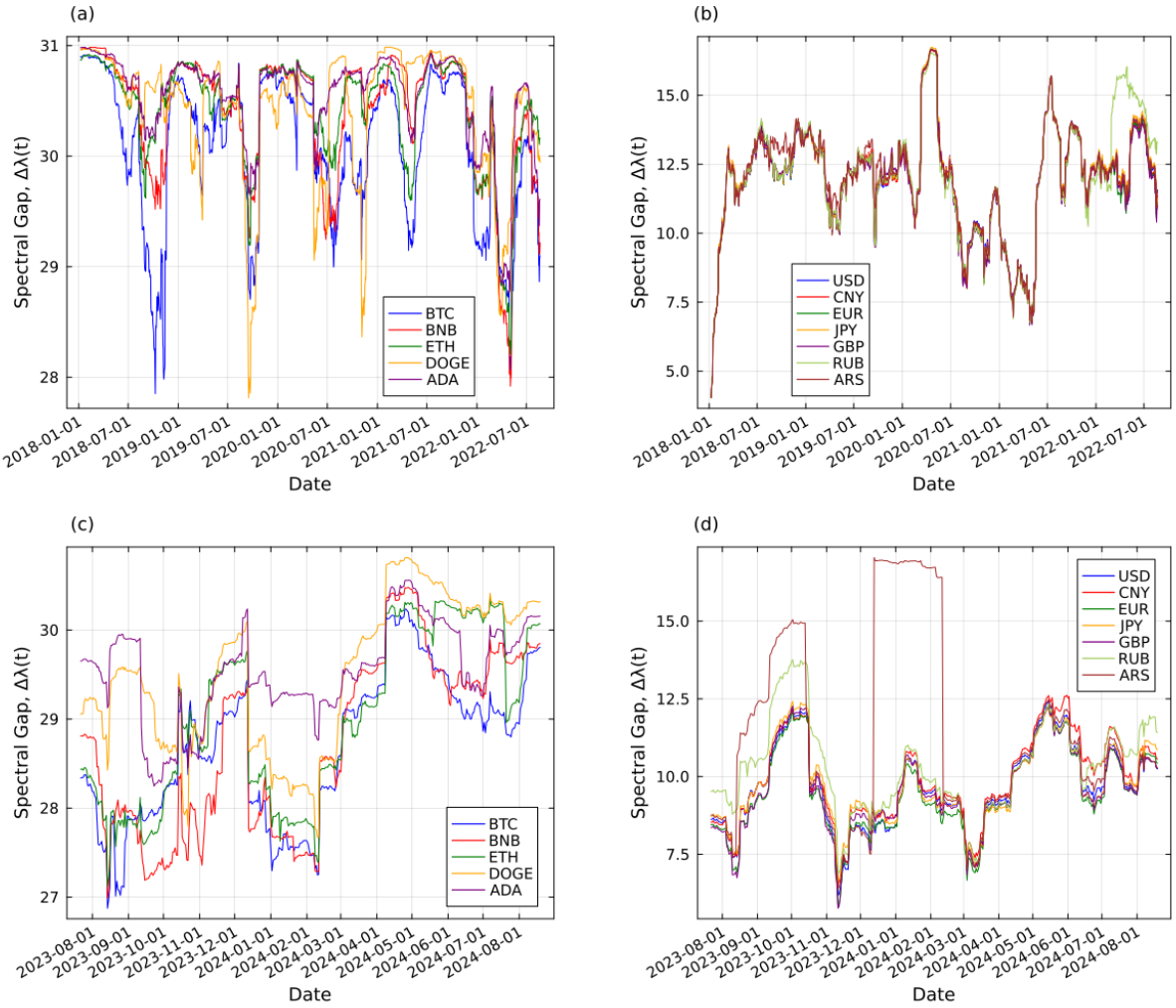

Fig. 9: Moving spectral gap analysis computed by fixing the reference (either crypto or fiat) in the correlation matrices. Panels (a) and (c) display the spectral gap when the crypto side is fixed, while panels (b) and (d) show the spectral gap when the fiat side is fixed, for the historical and recent datasets, respectively. (Ensure the labels match the actual panel content; adjust if file names imply the opposite.)

Appendix A: Appendix: List of Cryptocurrencies and Fiat Currencies Used

In this study, we analyze data from various cryptocurrencies and fiat currencies. The following is the complete list of assets considered in alphabetical order of their abbreviation.

- **Cryptocurrencies:** Cardano (ADA), Bitcoin Cash (BCH), Binance Coin (BNB), Bitcoin (BTC), Dash (DASH), Dogecoin (DOGE), EOS.IO (EOS), Ethereum Classic (ETC), Ethereum (ETH), Lisk (LSK), Litecoin (LTC), Neo (NEO), Omg network (OMG), TRON (TRX), NEM (XEM), Stellar (XLM), Monero (XMR), Ripple (XRP).
- **Fiat Currencies:** United Arab Emirates Dirham (AED), Argentina Peso (ARS), Australia Dollar (AUD), Bahrain Dinar (BHD), Brazil Real (BRL), Canada Dollar (CAD), Swiss Franc (CHF), Chinese Yuan (CNY), Czech Koruna (CZK), Denmark Krone (DKK), Euro (EUR), British Pound Sterling (GBP), Hong Kong Dollar (HKD), Indonesia Rupiah (IDR), India Rupee (INR), Japanese Yen (JPY), South Korea Won (KRW), Sri Lanka Rupee (LKR), Mexico Peso (MXN), Malaysia Ringgit (MYR), Nigeria Naira (NGN), Norway Kroner (NOK), New Zealand Dollar (NZD), Poland Zloty (PLN), Russia Rouble (RUB), Sweden Krona (SEK), Singapore Dollar (SGD), Turkish New Lira (TRY), Ukraine Hryvnia (UAH), United States Dollar (USD), and South Africa Rand (ZAR).

All currency symbols and abbreviations follow the standard ISO 4217 codes for fiat currencies and commonly accepted ticker symbols for cryptocurrencies.

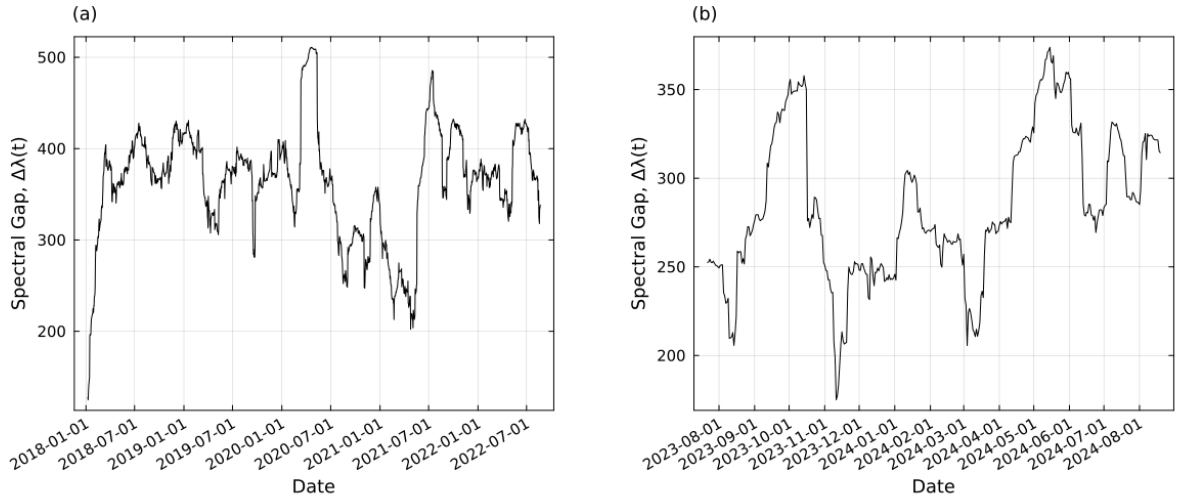

Fig. 10: Time evolution of the total spectral gap of the correlation matrices. Panel (a) shows the moving total spectral gap for the historical ("old") dataset, whereas panel (b) presents the corresponding evolution for the recent dataset. These plots highlight changes in the overall structure and collective dynamics of the crypto–fiat market over time.

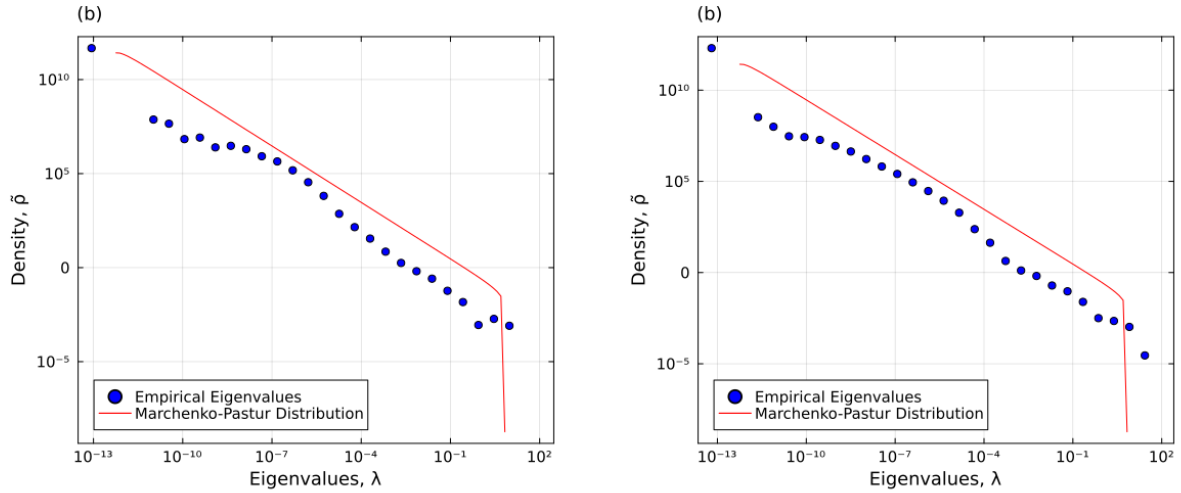

Fig. 11: Theoretical and Empirical eigenvalues of the random part of (a) old data, (b) newer data

References

1. C.W.J. Granger, *Proceedings*, api.semanticscholar.org, CorpusID:41012146,(1969)
2. T. Schreiber, Phy. Rev. Lett. **85**, (2000)
3. M. Reza R. Tabar, F. Nikakhtar, L. Parkavousi, A. Akhshi, U. Feudel, K. Lehnertz, Phys. Rev. X, (2024)
4. J. Karvanen, *Proceedings*, api.semanticscholar.org, CorpusID:18288903, (2003)
5. P. Folgueras, S. Solari, M. Mier-Torrecilla, M. Doblaré, M.A. Losada, J. Wind Eng. Ind. Aero. **157**, (2016)
6. V.M. Artyushenko, V. I. Volovach, Informacionno-Technologicheskij Vestnik, (2019)
7. L.H.S. Fernandes, W.D. Kristjanpoller, B.M. Tabak, Fractals, (2022)
8. W. Zhang, P. Wang, X. Li, and D. Shen, Complexity, (2018)
9. J. Fernández-Macho, Res. Meth. & Methodology Account. eJ., (2017)
10. S. Micciche,*Proceedings*, api.semanticscholar.org, CorpusID:269921144 (2024)
11. V.L. Girko, A.K. Gupta, *Proceedings*, api.semanticscholar.org, CorpusID:121223812, (1994)
12. S. Pueyo, *Proceedings*, api.semanticscholar.org, CorpusID:120512135, (2013)
13. M.R.R. Tabar, *Analysis and data-based reconstruction of complex nonlinear dynamical systems*, Springer Cham, (2019)

14. M.C. Münnix, T. Shimada, R. Schäfer, F. Leyvraz, T.H. Seligman, T. Guhr, H.E. Stanley, *Identifying States of a Financial Market*, Scientific Reports, vol. 2, (2012)
15. O. Bohigas, M.J. Giannoni, *Proceedings*, api.semanticscholar.org, CorpusID:120589647 (1975)
16. J.-P. Bouchaud, M. Potters, *Proceedings*, api.semanticscholar.org, CorpusID:167088876 (2000)
17. Y. Malevergne, D. Sornette, Capital Markets: Asset Pricing & Valuation, (2002)
18. Y. Malevergne, D. Sornette, Quant. Finance, **3**, (2001)
19. R.N. Mantegna, Cond. Matt. Complex Sys. **11**, (1998)
20. S. Nakamoto, dx.doi.org/10.2139/ssrn.3440802, (2008)
21. A.H. Dyhrberg, Finance Res. Letters, **16**, (2016)
22. K.John, L.Kogan, F. Saleh, Annual Rev. Financ. Eco. **15**, (2023)
23. R. van Eekeren, Inter. Rel.: Global Polit. Eco. (2021)
24. V. Plerou, P. Gopikrishnan, B. Rosenow, L.A.N. Amaral, T. Guhr, H.E. Stanley, Phys. Rev. E, **65**, (2002)
25. R. Cont, Quant. Finan. **1**, (2001)
26. G.-J. Wang, C. Xie, H.E. Stanley, " Comput. Econ. **51**, (2018)